Glycerol dehydration to hydroxyacetone in gas phase over copper supported on magnesium oxide (hydroxide) fluoride catalysts

Stephane Celerier, Sophie Morisset, Isabelle Batonneau-Gener, Thomas Belin, Khaled Younes, Catherine Batiot-Dupeyrat

Glycerol dehydration to hydroxyacetone in gas phase over copper supported on magnesium oxide (hydroxide) fluoride catalysts

Stéphane Célerier, Sophie Morisset, Isabelle Batonneau-Gener, Thomas Belin, Khaled Younes and Catherine Batiot-Dupeyrat*

IC2MP, UMR CNRS 7285, ENSIP, Université de Poitiers, 1 rue Marcel Doré, 86022 Poitiers,

*Corresponding author: catherine.batiot.dupeyrat@univ-poitiers.fr, Phone: +33549453898,

Abstract:

The dehydration of glycerol to hydroxyacetone was studied over copper-based catalysts using magnesium oxide (hydroxide) fluoride with various F/Mg ratio as support of copper. After calcination at 350°C, the incorporation of copper, mainly at + II oxidation state, into the support lattice was observed for MgO and MgF(OH) while copper was stabilized as Cu^{+1} at the surface of Cu-MgF_2. The reaction of dehydration was performed using a mixture of glycerol and water (80%wt of glycerol), in gas phase at 260°C. Cu-MgF_2 was the most active catalyst with a yield in hydroxyacetone of 45.5%, while the catalytic activity was very low for Cu-MgF(OH) and Cu-MgO (yield in HA <10%). Moreover, the performances obtained for Cu-MgF_2 were higher than those obtained with La_2CuO_4, a reference catalyst. After four hours of reaction, Cu-MgF_2 was not significantly modified, while for the two other catalysts, Cu^{2+} initially present was reduced into metallic copper. The results obtained revealed that the basic properties of the catalysts did not govern the reaction of dehydration of glycerol into HA. The best catalyst (Cu-MgF_2) was the one possessing the higher amount of Lewis acid sites, and stabilizing copper at +1 oxidation state.

Introduction

Glycerol, the main byproduct obtained from biodiesel industry, is a very promising platform building blocks for fuels and chemicals production [1]. Many applications of glycerol valorization were reported in the literature, such as hydrogenolysis of glycerol to propanediols [2-4], dehydration to acrolein [5-8] and reforming to hydrogen or syngas [9]. Glycerol conversion into acrolein was successfully performed over solid acid catalysts such as heteropoly acids [10] or zeolites [11]. The formation of acrolein is often accompanied by the presence of hydroxyacetone.

Hydroxyacetone (HA) is an interesting chemical product used as flavour in food industry, dyes or additive in cosmetics. It is also an intermediate in the production of valuable compounds such as propyleneglycol, acrolein or propionaldehyde. Therefore there are needs to develop active catalysts to produce selectively HA under mild experimental conditions, in a fixed bed continuous flow process at atmospheric pressure. Indeed, heterogeneous catalytic processes allow to avoid commonly encountered drawbacks of homogeneous catalytic processes including the difficulty of catalysts separation and problems of waste disposal.

Hydroxyacetone can be obtained from glycerol dehydration in gas phase, over catalysts containing Lewis acid sites such as MOx-Al_2O_3-PO_4 [12] or Zn-Cr oxides [13] or catalysts containing basic sites such as $NiCo_2O_4$ [14] while over strong Bronsted acid sites the formation of acrolein is favoured [15]. High selectivity to HA was also achieved using the 5%Na doped CeO_2 basic catalyst at 350°C, but a poor stability was observed with a rapid deactivation with time on stream [16].

Copper-based catalysts were widely used to perform the hydrogenolysis of glycerol to propanediols due to their lower price and higher resistance to poisoning than noble metals [17]. Copper was also preferred to nickel or cobalt due to its lower activity for C-C bond cleavage. Layered double hydroxide (LDH) supported Cu catalysts were successfully used in

the hydrogenolysis of glycerol in aqueous solution, under hydrogen pressure. The high activity was attributed to the strong basicity of the catalyst [18]. For the hydrogenolysis of glycerol, copper is used in its reduced form (Cu°) in order to favour the hydrogenation step which follows the dehydration one at the surface of the oxide support. Moreover it is also proposed that the Cu metallic site is involved in the dehydrogenation of glycerol to glyceraldehyde, followed by its dehydration and subsequent hydrogenation to HA [1]. Copper based catalysts were also successfully used without reduction for low temperature glycerol conversion to lactic acid in liquid phase under alkaline conditions [19]. The main drawbacks of the reaction performed in liquid phase are the use of relatively high temperatures and pressures requiring expensive equipments.

In the past decade, metal fluorides and oxide (hydroxide) fluorides prepared by soft chemistry, exhibiting tunable acid-base properties and high specific surface area, have shown promising results in different heterogeneous catalytic processes as active phase or support [20,21]. More specifically, magnesium fluoride was used successfully as support for numerous reactions such as CO oxidation [22], DeNOx [23] synthesis of menthol [24], alkylation of thiophenic compounds [25], synthesis of furfural [26], hydrogenation [27] among others, due to its high thermal and chemical stability. MgF_2 is considered as an inert support [28] or as an active support with high density of acid sites with moderate strength [29, 30], depending on the specific surface area and thus, on the synthesis process. Magnesium oxide (hydroxide) fluorides $MgF_{2-x}O_{x/2}$ (or $MgF_{2-x}(OH)_x$) or, more specifically, the intimate mixture with controlled composition of MgO and MgF_2, formed after calcination above 400°C, were also successfully used as support in several applications [31, 32]. The synthesis and characterization of this new Mg–O–F system and its application as catalytic support were described [33-35]. As an example, MgF_2–MgO can be considered as a potential support of NiO in NOx reduction by propene [33]. The synthesis of the MgF_2–MgO mesoporous

material, particularly by sol-gel method [31,36], allows to increase the specific surface area compared to single MgF_2, MgO or $Mg(OH)_2$ whatever the temperature of calcination [36]. For example, a specific surface area of 644 $m^2.g^{-1}$ can be obtained for MgF(OH) before calcination whereas the specific surface area of MgF_2 is of 231 $m^2.g^{-1}$ in the same synthesis conditions. The higher specific surface area favors the high dispersion of the active phase at the surface of the support, leading to high activity in several applications [31-34]. Moreover, the easy control of the F/Mg ratio, by sol-gel process, allows to fine tune the acid-base properties. Indeed, higher the fluorine content, higher the strength of Lewis acidity and lower the amount and strength of basicity [37]. This is obviously due to the stronger inductive effect of fluorine atom in comparison with oxygen atom. The interest of such materials was already demonstrated for Michael addition reactions [38]. Among the different soft chemistry method used to synthesize metal fluorides, the sol-gel method is very promising because it is simple, flexible and cheap, offering an easy control of porosity and microstructural properties [20].

In this work, the selective production of HA from glycerol in gas phase using magnesium oxide (hydroxide) fluoride as support of copper catalyst is reported. To the best of our knowledge, there is no report on the use of such materials for glycerol conversion. A mixture of glycerol and water (80wt % glycerol) was used while the reaction temperature was fixed at 260°C. For comparison, a La_2CuO_4 catalyst was also evaluated as a reference catalyst, since we showed in a previous study that a high catalytic activity can be reached using pure glycerol (99.9%) [39]. A correlation between the properties of the materials (acid-base, oxidation state of copper) and HA yield is discussed.

Experimental

Catalyst synthesis

The oxide (hydroxide) fluoride materials used in this work were prepared by a sol-gel method, partly based on the work of Scholz et al. [36]. In a first step, magnesium metal (3.23g, Aldrich, 99,98%) was treated with methanol in excess (100 mL, Sigma-Aldrich, 99,8%) under reflux conditions for 6 h to form a $Mg(OCH_3)_2$ metal alkoxide solution. For MgF_2 support, stoichiometric amount of aqueous HF (11.074 g, 48 wt% HF in water) was added progressively to the solution under stirring (avoiding the formation of a gel). A highly exothermic reaction proceeds leading to the formation of a sol. This sol was stirred for 24 h, aged at ambient temperature for 24 h, and dried at 100°C for 24 h, leading to the formation of the powder named MgF_2. For the support named MgF(OH), the protocol was the same except the added amount of HF, which was adjusted to obtain an initial F/Mg ratio of 1. Additional water was used for the hydrolysis of remaining $-OCH_3$ groups, to form hydroxyl group (hydrolysis reaction). For the support named MgO, no HF was added and the hydrolysis reaction was carried out with an excess of water (6 g, H_2O/Mg = 2.5). After drying at 100°C, the materials were calcined at 350°C for 5 h under dry air.

For the impregnation of copper on the support, 2 g of powder were mixed with a copper acetate solution: 330.5 mg of $(CH_3COO)_2Cu.1H_2O$ (Aldrich, 98%) dissolved in 17 mL of water. The amount of copper precursor was adjusted to obtain a theoretical weight content of metallic copper of 5 %. This mixture was stirred for 24 h, at ambient temperature and dried at 100°C on a sand bath followed by a final drying in a furnace at 80°C for 12 h. The catalysts were then calcined at 350°C, for 5 hours, under dry air to form copper oxide, the materials are named Cu-MgO, Cu-MgF(OH) and Cu-MgF_2.

In order to compare the performances of these new catalysts with a reference catalyst, La_2CuO_4 was also prepared as described in ref [39].

Characterization

XRD analysis of samples were carried out with a PANalytical EMPYREAN powder diffractometer using CuK_α radiation source (K_{α_1} = 1.5406 Å and K_{α_2} = 1.5444 Å). XRD patterns were collected between 15 and 80° with a 0.033° step and 300 s dwell time at each step. The identification of the phases was performed with the HighScorePlus software (PANalytical©) and by comparison with the ICDD database reference files.

Nitrogen adsorption was performed at -196°C using a TRISTAR 3000 gas adsorption system. Prior N_2 adsorption, the powder samples were degassed under secondary vacuum for 12 h at 250°C. The BET equation was used to calculate the surface area of the samples (S_{BET} in $m^2.g^{-1}$). The total pore volume was calculated from the adsorbed volume of nitrogen at P/P_0 equal to 0.99. The average mesopore-size distribution was calculated from the desorption isotherm branch using the Barret-Joyner-Halenda (BJH) method.

The magnesium and copper contents of the samples were determined by Inductively Coupled Plasma-Optical Emission Spectrometry (ICP OES) using a PerkinElmer Optima 2000DV instrument.

The amount of carbon deposition, after the catalytic test, was calculated by Thermogravimetric analysis (TGA) using a Q600TA Instrument apparatus, under dry air, with a heating rate of 5 °C min^{-1} from room temperature to 900°C.

The acidity of solid materials was measured by adsorption of pyridine followed by FT-IR spectroscopy, using a ThermoNicolet NEXUS 5700 spectrometer with a resolution of 2 cm^{-1} and 128 scans per spectrum. The samples were pressed into thin pellets (10-30 mg) with diameter of 16 mm under a pressure of 1-2 $t.cm^{-2}$ and activated *in situ* during one night under vacuum (10^{-5} Pa) at 250°C. Pyridine was introduced in excess, at 150°C, after the activation period. The solid sample was vacuum-packed to eliminate physisorbed pyridine and IR spectrum was recorded at 150°C. The concentration of Lewis acid sites was determined from

the integrated area band located between 1445 and 1455 cm^{-1}, using 1.28 $cm.\mu mol^{-1}$ as molar extinction coefficient. Note that no Bronsted acid site was detected by this method on all samples (no band observed between 1540 and 1550 cm^{-1}).

Temperature programmed reduction analysis (TPR) were carried out in a Micromeritics Autochem 2910 equipment using 100 mg of catalyst. The experiments were performed using a 5 % H_2/Ar mixture, with a flow rate of 100$mL.min^{-1}$, while the temperature was raised at 5 °C min^{-1} from ambient to 900 °C, then maintained at this temperature for 30 min. Prior to the measurements, the samples were outgassed under helium at 350 °C for 8 h.

CO_2 adsorption experiments were performed to determine the basic properties of the catalysts. Adsorption equilibrium data were measured thermogravimetrically at 298 K using a symmetrical SETARAM microbalance. A weight of 10 to 15 mg of sample was outgassed under secondary vacuum at 573 K for 6 hours and then cooled down to 298 K prior to the sorption measurements. The temperature of the system is kept constant during analysis by a water circulation in the double wall of the analysis tube. The CO_2 pressure was then increased step by step in order to obtain the entire adsorption isotherm. For each uptake, the equilibrium was reached when the mass recorded versus time and the pressure were stable.

The XPS analysis were carried out with a Kratos Axis Ultra DLD spectrometer using a monochromatic Al Kα source (10mA, 15kV). The charge Neutraliser system was operated for all analysis. Instrument base pressure was 9 x 10^{-8} Pascal. High-resolution spectra were recorded using an analysis area of 300 µm x 700 µm and a 40 eV pass energy. These pass energies correspond to Ag 3d5/2 FWHM of 0.55 eV. Data were acquired with 0.1 eV steps. All the binding energies were calibrated with the Mg2p binding energy fixed at 50.7eV as an internal reference.

Catalytic activity

The reaction was performed using a mixture of glycerol and water (80%wt of glycerol) with a liquid flow rate of 0.04 $mL.min^{-1}$. The reactor was a quartz tube of 13mm i.d. and 400mm length. The catalytic decomposition of glycerol was carried out at atmospheric pressure by passing a continuous flow of 20% v/v glycerol solution in N_2 as the carrier gas over the catalyst bed (200mg). The Gas Hourly Space velocity was equal to 13.5 $L.h^{-1}.g^{-1}$. A two zone reactor was used, glycerol being vaporized in the first empty zone before arriving to the reaction zone.

The temperature in the first reactor was maintained at 300°C, while the temperature in the second reactor was fixed at 260°C. Liquid phase products were recovered by condensation in two cold traps located at the reactor outlet for further analysis, whereas gas phase was analyzed by gas chromatography during the reaction. We checked that under the experimental conditions used (relatively low temperature) no significant gaseous products such as carbon monoxide or carbon dioxide was produced. Separation and quantification of main organic compounds in liquid phase were performed using a gas chromatograph (Varian 430 GC) equipped with a capillary column (50 m x 0.25mm x 0.2 µm, CP WAX 58 CB) and a FID detector. Quantification was performed by using butanol as internal standard. The products of the glycerol decomposition were identified by GC-MS (Varian 3800, injector 1079) coupled with a mass spectrometer (Analyser triple quadrupole Varian 1200L with an electric impact source of 70eV).

Conversion of glycerol and selectivity to hydroxyacetone was calculated according to the following equations:

$$\text{Glycerol conversion (\%)} = \frac{\text{mol of glycerol reacted}}{\text{mol of glycerol in the feed}} \times 100$$

$$\text{Selectivity to hydroxyacetone (\%)} = \frac{\text{mol of hydroxyacetone produced}}{\text{mol of glycerol transformed}} \times 100$$

Results and discussion

Synthesis and characterization of the catalysts

The different magnesium oxide (hydroxide) fluorides were prepared according to a sol-gel method, from a metal alkoxide precursor, in an aqueous HF solution. Briefly, a competition between fluorolysis (reaction with HF) and hydrolysis (reaction with water) occurs, resulting in the formation of $MgF_{2-x}(OH)_x$ as described in ref [36]. Kinetically, the fluorolysis rate is higher than the hydrolysis rate, allowing a partial control of the composition. As reported previously, with an equivalent method [36], the final F/Mg ratio (2-x) corresponds approximately to the initial HF/Mg ratio. The remaining -OCH_3 groups of the magnesium alkoxide react with water forming the hydroxyl groups of the hydroxide fluorides. Based on previous works [36], materials with a composition closed to MgF_2 (x = 0), MgF(OH) (x = 1) and $Mg(OH)_2$ (x = 2) were synthesized with an initial HF/Mg ratios of 2, 1 and 0 respectively. Thus, the fluorine content in the magnesium hydroxide fluoride is easily tuned thanks to the amount of HF added [31].

The X-ray diffraction (XRD) patterns of Cu-MgO, Cu-MgF(OH) and Cu-MgF_2 obtained after copper impregnation on the magnesium oxide hydroxide fluoride supports, and after calcination at 350°C are reported in Figure 1. The calcination temperature was chosen in order to stabilize thermally the catalysts while the reaction was performed at 260°C. MgO (card n°01-089-7746 of the ICDD database), MgF_2 (card n°98-009-4270) and a mixture of $Mg(OH)_2$ (card n°01-075-1527) and MgF_2 are mainly observed on the samples Cu-MgO, Cu-MgF_2 and Cu-MgF(OH) respectively. Interestingly, MgO in Cu-MgO and MgF_2 in Cu-MgF_2 are well crystallized whereas a low degree of crystallinity is observed for Cu-MgF(OH). Indeed, the presence of two phases affects the rate of crystallization of both phases as observed by Wojciechowska et al. [23]. In our experimental conditions, the method used does

not lead to the formation of a magnesium oxide (hydroxide) fluoride but to an intimate mixture of magnesium oxide (or hydroxide in our case) and fluoride as already observed in previous works [23]. The formation of CuO (card n°00-041-0254) with the main diffraction peaks at 35.5 and 38.8° and Cu_2O (card n°98-005-2043) with the main diffraction peaks at 36.4 and 42.3° are clearly observed for Cu-MgO and Cu-MgF_2 respectively. Nevertheless, the presence of CuO on Cu-MgF_2 and Cu_2O on Cu-MgO cannot be totally excluded due to the overlapping of copper oxide with the peaks of the support. The attribution of the copper phase is more difficult in the case of Cu-MgF(OH). Only one peak at 36.1 can be attributed to copper oxide phase. Nevertheless, this broad peak with low intensity, characteristic of poorly crystallized phase, can be attributed to (111) peak of CuO as well as (111) peak of Cu_2O since the other main peaks of these phases can be overlapped with the broad peaks of $Mg(OH)_2$ and/or MgF_2.

Finally, due to the low intensity of copper phases on XRD patterns, the determination of the crystallite size of copper oxide is difficult. Nevertheless, the higher intensity and thinner peaks of Cu_2O in Cu-MgF_2 is characteristic of larger crystallites in comparison with copper oxides in Cu-MgO and Cu-MgF(OH).

The copper contents determined by ICP OES analysis (Table 1) are closed to the desired theoretical content (5%) indicating that the chosen synthesis method is well adapted to control the copper content.

The specific surface areas of the samples are reported in Table 1. As observed, after calcination at 350°C and before impregnation of copper, the MgF(OH) support possesses a very high specific surface area (270 $m^2.g^{-1}$), higher than the S_{BET} of MgO (227 $m^2.g^{-1}$) and especially the S_{BET} of MgF_2 (33 $m^2.g^{-1}$). This result confirms that the synthesis of magnesium oxide (hydroxide) fluoride (or the intimate mixture of MgF_2 and $Mg(OH)_2$ in our case) by sol-gel method, improves the specific surface area compared to MgF_2 and MgO alone. This can

be attributed to the low rate of crystallinity of this sample as discussed above. The adsorption-desorption isotherms of all solids are shown in Fig. S1 (see supplementary information). A type IV isotherm according to the IUPAC classification was observed for all samples, whatever the fluorine content, showing the formation of mesoporous solids with high value of porous volume (Table S1). The porous volume decreases with the increase of fluorine content. The average pore size is significantly smaller for the MgF(OH) support in comparison with MgF_2 and MgO.

After impregnation of copper and calcination at 350°C, the specific surface area decreases for Cu-MgF(OH) from 270 to 165 $m^2.g^{-1}$ and for Cu-MgO from 227 to 68 $m^2.g^{-1}$, whereas it remains stable for Cu-MgF_2 with 33 $m^{2\cdot}g^{-1}$ before and 36 $m^{2\cdot}g^{-1}$ after copper impregnation and calcination. A type IV isotherm is retained for the three catalysts (Fig S1), the pore volume decreases for Cu-MgF(OH) and for Cu-MgO in comparison with the supports without copper, which is in accordance with the changes of specific surface area. The average pore sizes are retained before and after copper impregnation and calcination (table S1). The decrease of the specific surface area can be attributed to the impregnation step performed in water, with a probable hydrolysis of the remaining $–OCH_3$ due to the incomplete fluorination/hydrolysis of the methanolic $Mg(OCH_3)_2$ solution [40]. Indeed, the higher the content of the remaining –OR in the magnesium oxide (hydroxide) fluoride, the larger the surface. Nevertheless, very high specific surface area is obtained for Cu-MgF(OH) compared to the two other samples which is in accordance with the low rate of crystallinity observed by XRD (Fig. 1).

The determination of the acidity of the catalysts was performed by adsorption of pyridine followed by FT-IR spectroscopy and the results are reported in Table 1 and fig S2. A deeper discussion is also reported in section 2 of the supplementary information concerning the experiments. Note that the characterization of the acidity of La_2CuO_4 catalyst was not possible due to the too low surface area of the catalyst (S_{BET}= 2.2 $m^2.g^{-1}$), that did not allow

the quantification of acid sites. No significant amount of Lewis acid site is observed on Cu-MgO and Cu-MgF(OH) by this method. On the contrary, a significant amount of Lewis acid sites (50 μmol g^{-1}) is determined on Cu-MgF_2. Interestingly, this value is closed to the amount observed on the support alone prepared at 350°C (48 μmol g^{-1}) showing that the presence of copper does not change significantly the acidity of the material (section 2 of supplementary information). This could be explained by the replacement of a Lewis acid site of MgF_2 by copper ion (+1), which acts as an electron acceptor providing Lewis acid centers [40]. However, it is also possible to propose that the Lewis acidity would result mainly from the support since Cu^{+1} is present as large particles at the surface of the support (according to XRD). Moreover, it is also possible that the Lewis acid sites of Cu^{+1} are not enough strong to react with pyridine.

Furthermore, it is well known that the strength of Lewis acid sites of MgF_2 is moderate [29]. For the supports MgO and MgF(OH), exhibiting no significant amount of Lewis acid sites (but basic properties, as discussed below), the introduction of copper did not enhance the number of Lewis acid site. The low acidity of CuOx-MgO catalysts was proved by Popescu et al. [41]. It could also be explained by the diffusion of copper into the basic support as shown by XPS (see below). Surprisingly, no Lewis acid sites are observed on Cu-MgF(OH) whereas MgF_2 is present in this sample (as shown by XRD). This can be explained by the formation of an intimate mixture of MgF_2 and $Mg(OH)_2$ leading to strong interactions between both phases. The presence of hydroxyl groups ($Mg(OH)_2$) in the vicinity of unsaturated magnesium Lewis acid sites (MgF_2) decreases probably the strength of Lewis acidity due to the lower inductive effect of -OH in comparison with fluorine atom. Consequently, the Lewis acid sites of Cu-MgF(OH) are not enough strong to react with pyridine, a strong base.

TPR analysis

The TPR profiles of the catalysts Cu-MgO, Cu-MgF(OH) and Cu-MgF_2 are reported in Fig. 2.

The reduction profile of Cu-MgO shows two broad peaks in the 250-500°C temperature range, which is in accordance with the results reported by Reddy et al. [42]. The first reduction peak can be attributed to the reduction of well distributed CuO species or small copper oxide clusters interacting weakly with the support, and the second reduction peak, at higher temperature can be associated to large CuO particles or aggregated CuO clusters [42, 43]. Moreover, the reduction of CuO in two steps was also proposed ($CuO \rightarrow Cu_2O \rightarrow Cu°$) [41].

The reduction of Cu-MgF_2 proceeds at low temperature (225°C) as a single peak, however the non-gaussian profile of the peak suggests that different copper oxide species are present. As shown in Fig. 1, Cu_2O particles are observed in Cu-MgF_2. According to previous studies, CuO is more easily reduced than Cu_2O, which seems in contradiction with the present study [44, 45] by example the reduction peak of CuO/SiC is centered at 287°C against 302°C for Cu_2O/SiC [44]. However the reduction temperature depends strongly on the nature of copper support. The reduction of Cu_2O at a temperature as low as 225°C was reported by different authors over TiO_2 [46, 47]. It was also shown that the reduction temperature depends strongly on phase structures: the Cu_2O-rutile TiO_2 interaction was much stronger than the Cu_2O-anatase TiO_2 interaction. In our case, weak Cu_2O interaction was observed with MgF_2 possessing the biggest particles and lower specific surface area.

The amount of H_2 consumed is reported in Table 2 for each catalyst. It can be observed that the hydrogen consumption for the reduction of Cu-MgO is significantly higher than that for the reduction of Cu-MgF(OH) and Cu-MgF_2. Assuming that the hydrogen consumption corresponds to copper oxide reduction, the amount of copper at the oxidation state of +2 and +1 can be calculated according to the following reactions:

$CuO + H_2 = Cu + H_2O$

$Cu_2O + H_2 = 2Cu + H_2O$

The results show that Cu^{2+} is mainly obtained on MgO while Cu^{1+} is the major copper species formed over MgF_2. This is in agreement with the characterizations by XRD exhibiting the presence of Cu_2O in Cu-MgF_2 and CuO in Cu-MgO. Thus, MgF_2, the more acidic support, stabilized copper species at +1 oxidation step, while a mixture of Cu^{2+} and Cu^{+} is obtained for MgF(OH). Obtaining a mixture of Cu^{2+} and Cu^{1+} for this last catalyst is not surprising since the support is composed of two intimately mixed phases (MgF_2 and $Mg(OH)_2$), each phase stabilizing Cu^{+} and Cu^{2+} respectively.

CO_2 adsorption isotherms for Cu-MgO, Cu-MgFOH and Cu-MgF_2 are used to characterize the basicity and are presented in figure 3. From the observed results, it appears that the material basicity is not linked to the copper content since the materials exhibit very different CO_2 adsorption behaviors. The total CO_2 adsorption capacity depends on the material porosity whereas the amount of CO_2 adsorbed in the monolayer is directly linked to the basic site number present at the material surface. So, these isotherms have been analyzed using the BET model. As expected, the calculated amount of CO_2 adsorbed in the monolayer is linked to the material BET surface area determined by nitrogen physisorption (figure 4). The more important the surface area is, the higher is the CO_2 amount directly in interaction with the solid surface. From these result, it appears that the Cu-MgFOH sample has the higher basic site amount and Cu-MgF_2 the lowest.

XPS analysis

The surface composition of the catalysts were determined by XPS analysis and the Cu/Mg atomic ratio was calculated. As shown in Table 3, the Cu/Mg ratio is higher at the surface of the MgF_2 support than in the bulk. In contrast, an important enrichment of Mg at

the surface of MgF(OH) and MgO is observed. The occupation of the catalyst surface by Mg was evidenced by Liu et al. studying a CuO-MgO-TiO_2 catalyst [48]. So, with MgF(OH) and MgO as support, copper is incorporated into the support lattice leading to a higher Cu-Mg interaction, which corroborates the TPR profiles. Using MgF_2 as support, the diffusion of copper into the bulk is not favored, the metal-support interaction is lower explaining the lower reduction temperature (see Fig. 2).

Cu 2p3/2 XPS spectra of the catalysts Cu-MgO, Cu-MgFOH and Cu-MgF_2 are shown in Figure 5. For the Cu-MgO catalyst, the presence of Cu^{2+} species is observed thanks to the presence of the satellites peaks (BE region between 938 eV and 944 eV) which is the fingerprint of Cu^{2+} oxidation state. However the binding energy corresponding to Cu 2p3/2 is observed at 932.9eV, a value significantly lower than the expected one: 933.6eV [49] probably due a charge transfer from the metal ion toward the support matrix.

For Cu-MgFOH, two Cu species seem to be present, one with a Cu 2p3/2 binding energy of 932.8 eV and the other with a Cu 2p3/2 binding energy of 936.1 eV. These are consistent with Cu(II) species and the latter is consistent with $Cu(OH)_2$ as proposed by Frost et al. [50]. Nevertheless the presence of CuF_2 cannot be excluded since fluoride atom are present in the support and can react with copper species. The formation of such species would confirm the reaction between copper and the support during the calcination step.

For the Cu-MgF_2 sample a single and intense peak centered at 932.1 eV is visible, while no satellite peaks are observed indicating that there is no Cu^{2+} but the presence of reduced copper species. As it is well known, XPS cannot differentiate between Cu^0 and Cu^+ since the binding energy is similar. However, the presence of Cu^0 is unlikely in the present study since the catalyst was calcined at 350°C under air and no metallic copper are observed by XRD.

The XPS analysis are in accordance with the results obtained by XRD and TPR, showing the presence of Cu^+ with MgF_2 used as support, while Cu^{2+} is formed on MgO. Moreover,

significant higher amount of copper is observed at the surface of MgF_2 compared to both other catalysts.

Consequently the combination of characterization methods (TPD, XRD, TPR, XPS), proves that copper is obtained at different oxidation state depending on the nature of the support. However it is not possible to propose a simple correlation between oxidation state of copper and support physico-chemical properties since the three materials differ strongly in terms of acid/base properties, fluorine content, size of particles…

Catalytic results

The reaction was investigated in gas phase using a mixture of glycerol and water (80 wt % glycerol) at 260°C to avoid the production of gaseous products at higher temperatures. The main product was HA but pyruvaldehyde and glyceraldehyde were also formed. Other products were analysed but they were present in low amount: propionaldehyde, glycidol, 1,3 propanediol, 1 propanol...

First, using the support alone (without copper) it was confirmed that no glycerol transformation occurs, indicating the crucial role of copper.

The catalytic activity of the copper supported on oxide (hydroxide) fluoride catalysts is compared with La_2CuO_4, which exhibited a high activity toward glycerol dehydration into hydroxyacetone in the absence of water in the gas feed [39]. The catalytic behavior of the three oxide (hydroxide) fluoride based catalysts differs strongly. The highest glycerol conversion is obtained over the Cu-MgF_2 catalyst, it reaches 82 % and remains relatively stable during four hours of reaction (figure 6). Cu-MgO and Cu-MgFOH are little active under our experimental conditions with a glycerol conversion of 19 % and 33 % after one hour of reaction respectively. The yield in HA is also maximum with Cu-MgF_2, decreasing

slightly with time on stream (figure 7). Moreover, the Cu-MgF_2 catalyst is significantly more active than La_2CuO_4, in the presence of water.

High glycerol conversions were also reported by Carvalho et al. [51] using Cu-based hydroyapatites. The authors showed that glycerol conversion increased with the amount of copper (from 3 to 17 %) highlighting the crucial role of copper as in the present work. However a catalytic deactivation is observed after few hours on stream. Sato et al. [52] studied the influence of the support on glycerol conversion over copper-based catalysts in gas phase at 250°C, they found that the acid-base property of the support affected the selectivity: basic MgO, CeO_2 and ZnO supports showed low selectivity to hydroxyacetone, while acidic supports such as Al_2O_3, ZrO_2, Fe_2O_3 and SiO_2 promoted HA selectivity which is in accordance with our results (Cu-MgF_2 being the most acidic catalyst).

Glycerol dehydration into hydroxyacetone implies the removal of one of the two OH groups from the terminal carbons in the glycerol molecule, while the removal of the OH group from the central carbon atom leads to the formation of acrolein through the unstable 3-hydroxypropenal. The predominant route depends mainly on the nature of the acid sites, it has been suggested that acrolein is formed over Brønsted acid sites and hydroxyacetone over Lewis acid sites [53]. The role of basic centers was also proposed by Stosic et al. [53]. The authors showed that the yield in HA was increased with the number of basic sites. However, using hydroxyapatite catalyst, the main reaction product was acrolein, they concluded that acrolein formation was not only controlled by the surface acidity but also by hindering the number/strength/activity of the basic sites, and thus limiting the side reactions which affect the selectivity in acrolein. An intermediate enol is suggested to be formed at the surface of basic centers, afterwards the enol is rapidly transformed by rearrangement into 1-hydroxyacetone. The results obtained in the present study showed that the basic properties of the catalysts does not governed the dehydration of glycerol into HA but that HA is

preferentially produced over the catalyst possessing Lewis acidity (Cu-MgF_2), while no acrolein was formed. The high yield in HA can be directly correlated with the amount of Cu^{+1}, which also corresponds to the maximum number of Lewis acid sites (figure 8). Moreover, the Lewis acid sites of the MgF_2 support are not able to convert glycerol into hydroxyacetone since no activity was observed with MgF_2 alone. Mitta et al. [40] also showed that a Y zeolite possessing 180µmol g^{-1} of Lewis acid sites exhibited a very low glycerol conversion without copper. It is thus possible to conclude that the dehydration of glycerol requires the presence of copper under the experimental conditions used (vapor phase, relatively low reaction temperature: 260°C in the present study and 210°C in the work of Mitta et al.).

The reaction route to hydroxyacetone involves the formation of an enol as proposed by different authors on copper based catalysts [54]. The important role of copper oxidation state was indicated by Pinheiro et al. [55] and Xiao et al. [56]. The weak acid sites, Cu^{2+} cannot be responsible for dehydration [57], as confirmed by the results we obtained in the present paper. It is also clear that metallic copper is an active site for dehydration of glycerol to HA, dehydrogenation at the surface of Cu° occurs first and the formation of Cu-alkoxide species is proposed [53, 58, 59]. Over Cu^{+}, the reaction mechanism is more difficult to establish, different authors showed that Cu^{+} is active for dehydration of glycerol [56, 57] which corroborates our results. Xiao et al. [56] indicate that it is not possible to state if Cu^{+} is active "per se" or if it is due to the Lewis acid properties of Cu^{+}.

So according to the studies published and to the results we obtained two different mechanisms are proposed: one based on Lewis acid properties of Cu^{+} and the other one based on the oxidation state of copper: Cu^{+}.

The involvement of the Lewis acid sites of Cu^{+} can be proposed according to the mechanism of Alhanash et al. (Fig.9 a). In the second mechanism, we propose a homolytic C-H bond

dissociation (similar to the one proposed on metallic copper, Fig.9 b). The C-H bond rupture at the surface of Cu^{+} is supported by the work of Wang et al. [60], who performed DFT calculations to explain the dehydrogenation of cyclohexanol to cyclohexanone. The authors proved that the hydrogen bonded to carbon is more easily removed on Cu^{+} than on Cu°, so a homolytic rupture of the C-H bond in glycerol by Cu^{+} is proposed.

In order to support the mechanism, theoretical calculations were performed and compared with the results of Nimlos [61] who established the more probable intermediate species in glycerol dehydration to HA. The calculations were performed at the B3LYP/6-31+G(d,p) level. Transition states took into consideration were radical intermediate of glycerol as shown in Fig. 9b. All computed energies of the mechanism compounds are Gibbs free energies at 534.15 K. Calculations were performed with the Gaussian09 code.

The relative energies of the transition states involved in the two mechanisms are 70.9 and 73.2 kcal/mol for mechanism 9a) and 9b) respectively (Fig. 10). Such high energy barriers indicate that these reactions are only likely to occur at high temperatures and under pyrolysis conditions. The values obtained, are in the same order indicating that the formation of intermediate species in the mechanism we propose are favorable in our experimental conditions (T=260°C).

Shortcomings of the simulation held should be highlighted, in our case we didn't take into consideration the "Transition State" theory as we considered each step of the mechanism as independent reactions. Additionally, the surface of the catalyst wasn't taken into consideration. This simplification hindered essential details about sorption and stabilization of glycerol on the surface.

Further studies on the theoretical and experimental level should be held on the role of the copper catalyst, and we consider that the discussion on the mechanism is still an open issue.

A low catalytic activity towards HA formation is observed with Cu-MgO and Cu-MgF(OH), which can result from low amount (or absence) of Cu^{1+} at the surface of the support and high amount of basic sites which probably favors the occurrence of side reactions giving by-products such as acids, aldehydes, aromatic compounds, glycerol oligomers [62]… and also coke as evidenced by TGA analysis (figure 11), as discussed below.

Characterization of the catalysts after reaction

After catalytic tests, the crystalline structure of the supports is retained (Fig. 1) showing the good stability of the magnesium oxide (hydroxide) fluoride materials under our experimental conditions, confirming their potential as support. The peaks corresponding to copper oxides disappear and the formation of metallic copper is observed on Cu-MgF(OH) and Cu-MgO. This result can be explained by the reduction properties of glycerol according to Jin et al. [63].

On the contrary, Cu_2O is always observed on Cu-MgF_2 even if the formation of Cu° cannot be totally excluded due to the peaks with very low intensity at 43.3° (shoulder) and 50.4° (figure 1). Moreover, the peaks of Cu_2O are broadened after reaction reflecting a decrease of the crystallites size probably due to a partial reduction of the oxide. Nevertheless, in our experimental conditions, MgF_2 support seems to stabilize the copper oxide at a degree of oxidation +I while metallic copper is obtained over the two other supports.

As observed in Table 1, the specific surface areas of Cu-MgF(OH) and Cu-MgO decrease drastically (from 165 to 17 $m^2.g^{-1}$ and from 68 to 37 $m^2.g^{-1}$ respectively) after catalytic tests whereas the specific surface area remains comparatively stable for Cu-MgF_2. This is in agreement with the XRD pattern since no change is observed after the catalytic test for Cu-MgF_2.

Thermal analyses (TGA) were performed on the catalysts before and after catalytic tests until 900°C (figure 11). As observed, a very weak weight loss (2.5%) is observed on Cu-MgF_2 corresponding to the removal of physisorbed water and/or remaining organic compounds derived from the sol-gel synthesis process. This weight loss is higher on Cu-MgO (4.7 %) and especially on Cu-MgF(OH) (14.6 %). In addition to physisorbed water and remaining organic compounds, these weight losses between 300 and 400 °C for Cu-MgO and between 400 and 500 °C for Cu-MgF(OH) can be explained by the dehydroxylation of magnesium hydroxide. This is in agreement with the XRD pattern of Cu-MgF(OH) (figure 1) showing the presence of magnesium hydroxide. Moreover, the XRD pattern of Cu-MgF(OH) after TGA (not shown) corresponds to a mixture of MgO and MgF_2 confirming this dehydroxylation. Even if only MgO is observed for Cu-MgO (figure 1), the presence of a small amount of hydroxyl group cannot be totally excluded. After catalytic tests, the weight losses are higher whatever the catalysts. This is due to the formation of "coke" on the catalyst during the transformation of glycerol, removed by oxidation during the thermal analysis under dry air. The deposition of coke is clearly limited on Cu-MgF_2 since the difference of weight loss before and after the catalytic test is only of 2.5 %. By contrast, the amount of coke is clearly higher for the two other catalysts with a difference of weight loss of 24 % for Cu-MgF(OH) and 12.9 % for Cu-MgO. These results are consistent with the S_{BET} which decreases after reaction for both catalysts while S_{BET} of Cu-MgF_2 remains stable as discussed above. Based on the assumption that basic sites play a role on the coke formation by side-reactions as discussed above, the amount of coke is also in accordance with basic properties, higher the basicity (figure 4), higher the amount of coke.

Thus, Cu-MgF_2 is a more suitable catalyst than the two other catalysts to avoid decrease of specific surface area, formation of coke and deactivation. Long terms experiment should be performed to confirm the catalytic stability of the catalyst.

Conclusions

The dehydration of glycerol to hydroxyacetone was successfully investigated over copper supported on magnesium oxide (hydroxide) fluoride catalysts, in gas phase in the presence of water at 260°C. The catalysts were prepared according to a sol-gel method following by a copper impregnation step and led to different CuO_x-magnesium oxide (hydroxide) fluoride composites with different crystallinities, copper oxidation state and tunable acid-base properties. Among the different studied catalysts, Cu-MgF_2 is the most interesting since Cu^+, the active site, is stabilized at the surface of the support, whereas no (or little) coke formation during time on stream is observed contrary to Cu-MgO and Cu-Mg(OH)F catalysts. Moreover, this catalyst led to the best catalytic activity and stability, with a glycerol conversion reaching 82% and a yield in hydroxyacetone of 45.5% after one hour of reaction. Cu-MgF_2 is much more active than La_2CuO_4 (26.7% yield in HA) which exhibited a high activity towards HA synthesis but in the absence of water. The results obtained in the present study showed that the basic properties of the catalysts did not governed the dehydration of glycerol into HA. The best catalyst (Cu-MgF_2) is the one possessing Lewis acidity and stabilizing copper at +1 oxidation state.

Thanks to their tunable properties (acid/base, specific surface area, metal/support interaction), this work confirms the potential of magnesium oxide (hydroxide) fluoride as support for different heterogeneous catalytic processes as already observed for other reactions. In another way, it offers new opportunities for the production of hydroxyacetone from glycerol with an environmentally friendly process.

References

[1] A. Behr, J. Eilting, K. Irawadi, J. Leschinski, F. Lindner, Green Chem., 10 (2008) 13-30

[2] D. Sun, Y. Yamada, S. Sato, W. Ueda, Appl. Catal. B: Env., 193 (2016) 75-92

[3] D. Roy, B. Subramaniam, R. V.Chaudhari, Catal. Today, 156 (2010) 31-37

[4] V. Montes, M. Checa, A. Marinas, M. Boutonnet, J.M. Marinas, F.J. Urbano, S. Järas, C. Pinel, Catal. Today, 223, (2014) 129-137

[5] M. Massa, A. Andersson, E. Finocchio, G. Busca, J Catal. 307 (2013) 170-184

[6] J. Deleplanque, J.-L. Dubois, J.-F. Devaux, W. Ueda, Catal. Today, 157 (2010) 351-358

[7] A. Talebian-Kiakalaieh, N. Aishah Saidina Amin, Renewable Energy, 114 (2017) 794-804

[8] T. Ma, J. Ding, R. Shao, W. Xu, Z. Yun, Chem. Eng. J., 316 (2017) 797-806

[9] M. E Doukkali, A. Iriondo, J.F. Cambra, I. Gandarias, L. Jalowiecki-Duhamel, F. Dumeignil, P.L. Arias, Appl. Catal. A: Gen. 472 (2014) 80-91

[10] M. Dalil, D. Carnevali, M. Edake, A. Auroux, J.L. Dubois, G.S. Patience, J. Mol. Cat. A: Chem., 421 (2016) 146-155

[11] L. H. Vieira, K.T.G. Carvalho, E. A. Urquieta-González, S . H. Pulcinelli, C. V. Santilli, L. Martins, J. Mol. Cat. A: Chem., 422 (2016) 148-157

[12] W. Suprun, M. Lutecki, H. Papp, Chem. Eng. Tech. 33 (2010) 1-7

[13] A. Alhanash, E. F. Kozhevnikova, I. V. Kozhevnikov, Appl. Catal. A: Gen., 378 (2010) 11-18

[14] C.L. Lima, S. J.S. Vasconcelos, J.M. Filho, B. C. Neto, M.G.C. Rocha, P. Bargiela, A. C. Oliveira, Appl. Catal. A: Gen 399 (2011) 50-62

[15] P. Lauriol-Garbey, J.M.M. Millet, S. Loridant, V. Bellière-Baca, P. Rey, J. Catal. 281 (2011) 362-370

[16] A. Kinage, P. Upare, P. Kasinathan, Y. Kyu Hwang, J.S. Chang, Catal. Comm. 11 (2010) 620-623

[17] C. Montassier, J.C. Ménézo, L.C. Hoang, C. Renaud, J. Barbier, J. Mol. Cat. 70 (1991) 99-110

[18] S. Xia, R. Nie, X. Lu , L.Wang, P. Chen, Z. Hou, J. Catal. 296 (2012)1-11

[19] D. Roy, B. Subramaniam, R. V. Chaudhari, ACS Catal. 1 (2011) 548-551

[20] E. Kemnitz, Catal. Sci. Technol. 5 *(*2015), 786-806

[21] S. Célérier F. Richard, Catal. Commun. 67 (2015) 26-30

[22] M. Wojciechowska, W. Przystajko, M. Zielinski, Catal. Today 119 (2007) 338–341

[23] M. Wojciechowska, M. Zielinski, M. Pietrowski, Catal. Today 90 (2004) 35–38

[24] A. Negoi, S. Wuttke, E. Kemnitz, D. Macovei, V. I. Parvulescu, C. M. Teodorescu, S. M. Coman, Angew. Chem. Int. Ed. 49 (2010)) 8134 –8138

[25] F. Richard, S. Célérier, M. Vilette, J. D. Comparot, V. Montouillout, Appl. Catal. B 152-153 (2014) 241-249

[26] I. Agirrezabal-Telleria, F. Hemmann, C. Jäger, P.L. Arias, E. Kemnitz, J. Catal. 305 (2013) 81–91

[27] M. Zielinski, M. Pietrowski, A. Kiderys, M. Kot, E. Alwin, J. Fluor. Chem. 195 (2017) 18–25

[28] M. Wojciechowska, M. Zielinski, M. Pietrowski, J. Fluor. Chem. 120 (2003) 1-11

[29] S. Wuttke, S. M. Coman, G. Scholz, H. Kirmse, A. Vimont, M. Daturi, S. L. M. Schroeder, E. Kemnitz , Chem. Eur. J. 14 (2008) 11488 – 11499

[30] E. Kemnitz, S. Wuttke, S. M. Coman, Eur. J. Inor. Chem., (2011) 4773-4794

[31] M. Wojciechowska, A. Wajnert, I. Tomska-Foralewska, M. Zielinski, B. Czajka, Catal Lett 128 (2009) 77–82

[32] I. Tomska-Foralewska, M. Zielinski, M. Pietrowski, W. Przystajko, M. Wojciechowska, Catal. Today 176 (2011) 263–266

[33] M. Zielinski, I. Tomska-Foralewska, M. Pietrowski, W. Przystajko, M. Wojciechowska, Catal. Today 191 (2012) 75–78

[34] M. Zielinski, A. Kiderys, M. Pietrowski, I. Tomska-Foralewska, M. Wojciechowska, Catal. Commun. 76 (2016) 54–57

[35] M. Bonarowska, M. Wojciechowska, M. Zielinski, A. Kiderys, M. Zielinski, P. Winiarek, Z. Karpinski, Molecules 21 (2016) 1620

[36] G. Scholz, C. Stosiek, M. Feist, E. Kemnitz, Eur. J. of Inorg. Chem. 14 (2012) 2337-2340

[37] S. Wuttke, S. M. Coman, J. Kroehnert, F. C. Jentoft, E. Kemnitz, Catal. Today 152 (2010) 2-10

[38] H. A. Prescott, Z. J. Li, E. Kemnitz, J. Deutsch, H. Lieske**,** J. Mater. Chem. 15 (2005) 4616–4628

[39] M. Velasquez, A. Santamaria, C. Batiot-Dupeyrat, Appl. Catal. B: Env, 160-161 (2014) 606-613

[40] H. Mitta, P. Kumar Seelam, S. Ojala, R. L. Keiski, P. Balla, Appl. Catal. A, General 550 (2018) 308-319

[41] I. Popescu, N. Tanchoux, D. Tichit, I.C. Marcu, Appl. Catal. A: Gen 538 (2017) 81-90

[42] K.H.P. Reddy, Y.W. Suh, N. Anand, B.D. Raju, K. S. Rama Rao, Catal. Com. 95 (2017)21-25

[43] M. Jablonska, L. Chmielarz, A. Wegrzyn, K. Guzik, Z. Piwowarska, S. Witowski, R.I. Walton, P.W. Dunne, F. Kovanda, J. Therm. Anal. Calorim. 114 (2013) 731-747

[44] Y. Wang, X. Guo, M. Lu, Z. Zhai, Y. Wang, X. Guo, Chinese Journal of Catalysis 38 (2017) 658-664

[45] C.S. Polster, H. Nair, C.D. Baertsh, J. Catal. 266 (2009) 308-319

[46] Y. Liu, Z. Wang, W. Huang, Appl. Surf. Sci. 389 (2016) 760-767

[47] C.S. Chen, T.C. Chen, C.C. Chen, Y.T. Lai, J.H. You, T.M. Chou, C.H. Chen, J.F. Lee, Langmuir, 28 (2012) 9996-10006

[48] C. Liu, X. Guo, Q. Guo, D. Mao, J. Yu, G. Lu, J. Mol. Cat. A: Chemical 425 (2016) 86–93

[49] M.C. Biesinger, L.W.M. Lau, A.R. Gerson, R.S.C. Smart, Appl. Surf. Sci. 257 (2010) 887–898

[50] Ray L. Frost, Yunfei Xi, Barry J. Wood, Thermochimica Acta 545 (2012) 157– 162

[51] D. C. Carvalho, L. G. Pinheiroa, A. Campos, E. R.C. Millet, F. F. de Sousac, J. M. Filhoc, G. D. Saraivac, E. C. da Silva Filhod, M. G. Fonsecae, A. C. Oliveira, Appl. Catal. A: Gen 471 (2014) 39-49

[52] S. Sato, M. Akiyama, R. Takahashi, T. Hara, K. Inui, M. Yokota, Appl. Catal. A : Gen 347 (2008) 186-191

[53] D. Stosic, S. Bennici, S. Sirotin, C. Calais, J.L. Couturier, J.L. Dubois, A. Travert, A. Auroux, Appl. Catal. A: Gen., 447-448 (2012) 124-134

[54] B. Katryniok, S. Paul, V. Bellière-Baca, P. Rey*e* and F. Dumeignil, Green Chem., 12 (2010) 2079-2098

[55] T.Pinheiro Braga, N. essayem, A. Valentini, J. Therm. Anal. Calorim. 129 (2017) 65-74

[56] Z. Xiao, X. Wang, J. Xiu, Y. Wang, C.T. Williams, C. Liang, Catal. Today, 234 (2014) 200-207

[57] P.A. Torresi, V.K. Diez, P.J. Luggren, J.I. Di Cosimo, Appl. Catalysis A: general 458 (2013) 119-129

[58] A.J. Gellman, M.T. Buelow, S.C. Street, T.H. Morton, J. Phys. Chem. A 104 (2000) 2476

[59] R.M. Rioux, M.A. Vannice, J. Catal. 216 (2003) 362-376

[60] Z. Wang, X. Liu, R. P. Hu, Surface Science 640 (2015) 181-189

[61] M.R. Nimlos, S.J. Blanksby, X. Qian, M.E. Himmel, D.K. Johnson, J.Phys. Chem. A 110 (2006) 6145-6156

[62] F.A.A. Barros, H.S.A. de Sousa, A . C. Oliviera, M.C. Junior, J.M. Filho, B.C. Viana, A.C. Oliveira, Catal. Today, 212 (2013) 127-136

[63] F. Jin, X. Zeng, Z. Jing, H. Enomoto, Ind. Eng. Chem. Res. 51 (2012) 9921-9937

Table 1 Textural properties of the catalysts

Support	**S_{BET} (m^2 g^{-1})**	**Catalyst**	**S_{BET} (m^2 g^{-1})**	**S_{BET} (m^2 g^{-1}) after catalytic test**	**Weight content of Cu (%)[1]**	**Lewis Acidity (µmol g^{-1})**
MgO	227	Cu-MgO	68	37	4.7	< 10
MgF(OH)	270	Cu-MgF(OH)	165	17	4.6	< 10
MgF_2	33	Cu-MgF_2	36	27	4.8	50
		La_2CuO_4	2.2	n.d.		

[1] determined from ICP OES analysis

Table 2 Hydrogen consumption and Cu^{2+}/Cu^{+} concentration determined from TPR analysis.

Catalyst	H_2 consumption for copper oxide reduction (mL STP/g) (± 2%)			Cu (%)***	
	Estimated* a) Cu^{2+}	b) Cu^{+}	Determined**	Cu^{2+}	Cu^{+}
Cu-MgO	21.5	10.7	20.5	91	9
Cu-MgF(OH)	19.5	9.8	16.3	67	33
Cu-MgF_2	20.3	10.2	12.7	25	75

*Estimated: calculated from the nominal composition of the material according to the following reactions: a) $CuO + H_2 = Cu + H_2O$ and b) $Cu_2O + H_2 = 2Cu + H_2O$

**Determined: obtained from H_2-TPR profile

*** Cu^{2+} and Cu^{+} concentration (%) estimated from the volume of H_2 obtained by TPR

Table 3 Cu/Mg atomic ratio

Atomic ratio Cu/Mg	Cu-MgO	Cu-MgF(OH)	Cu-MgF_2
Bulk*	0.036	0.050	0.054
Surface**	0.008	0.029	0.082

* Calculated from ICP OES

** Calculated from XPS analysis

Figure 1. XRD patterns of (I and I') Cu-MgO, (II) Cu-MgF(OH) and (III) Cu-MgF_2 after synthesis (a) and after catalytic test (b).

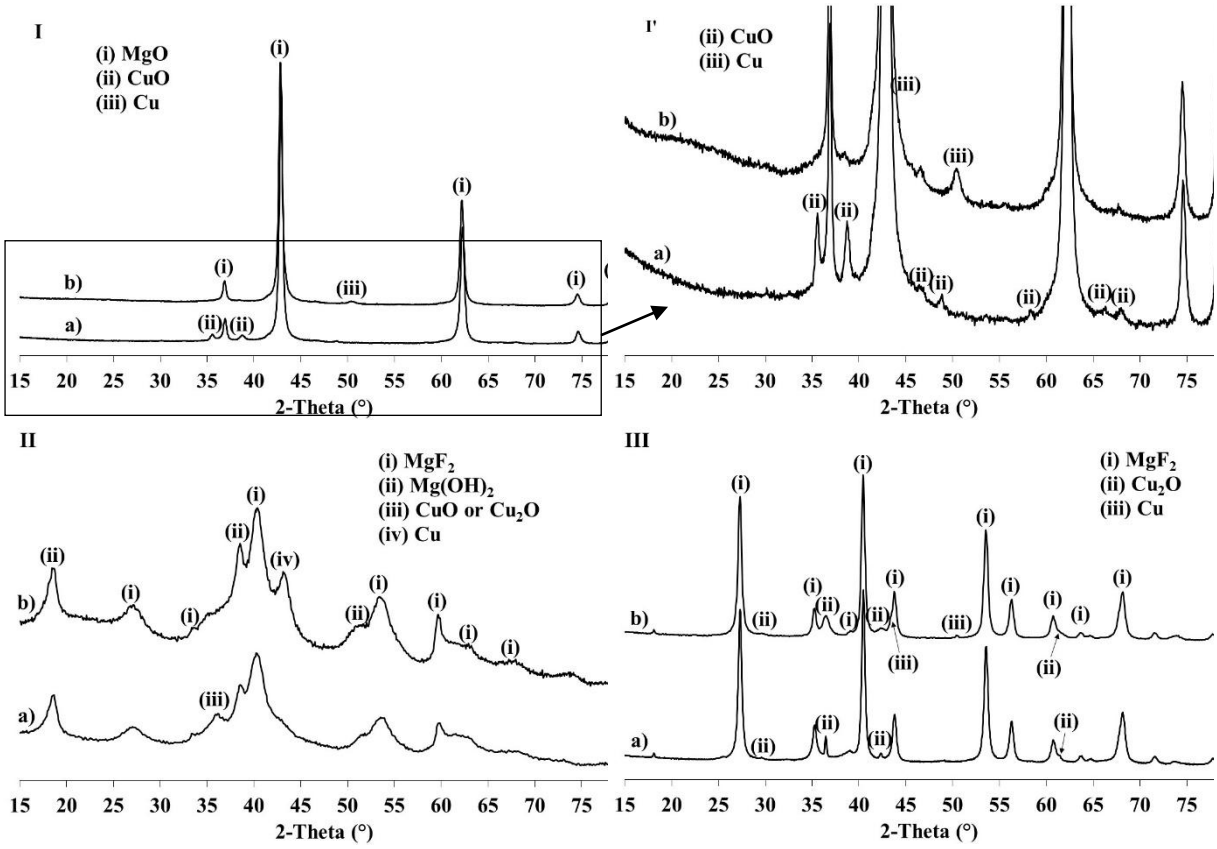

Figure 2: TPR analysis

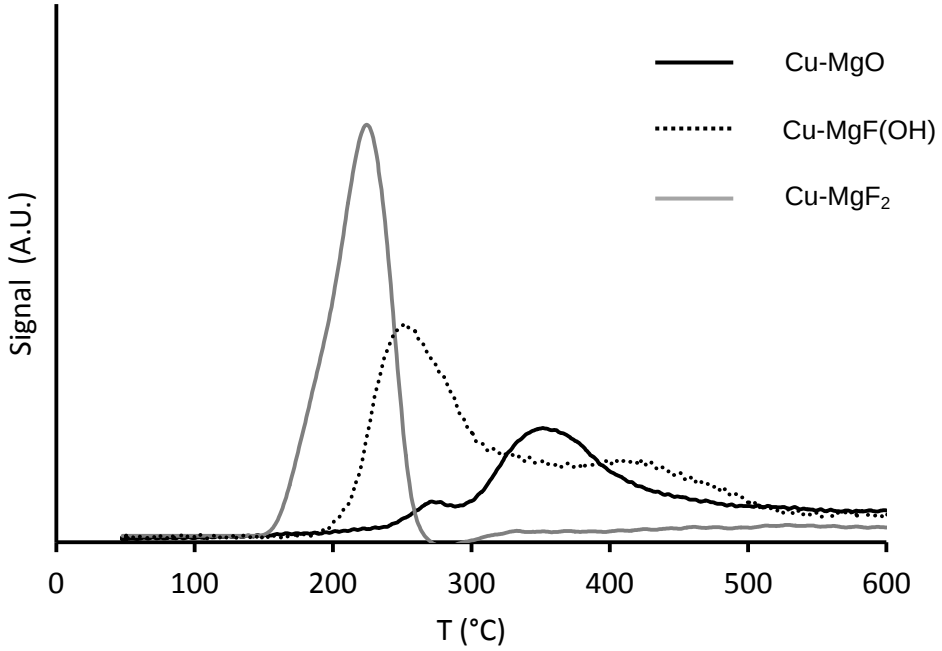

Figure 3: Isotherms of CO_2 adsorption on Cu-magnesium fluoride catalysts

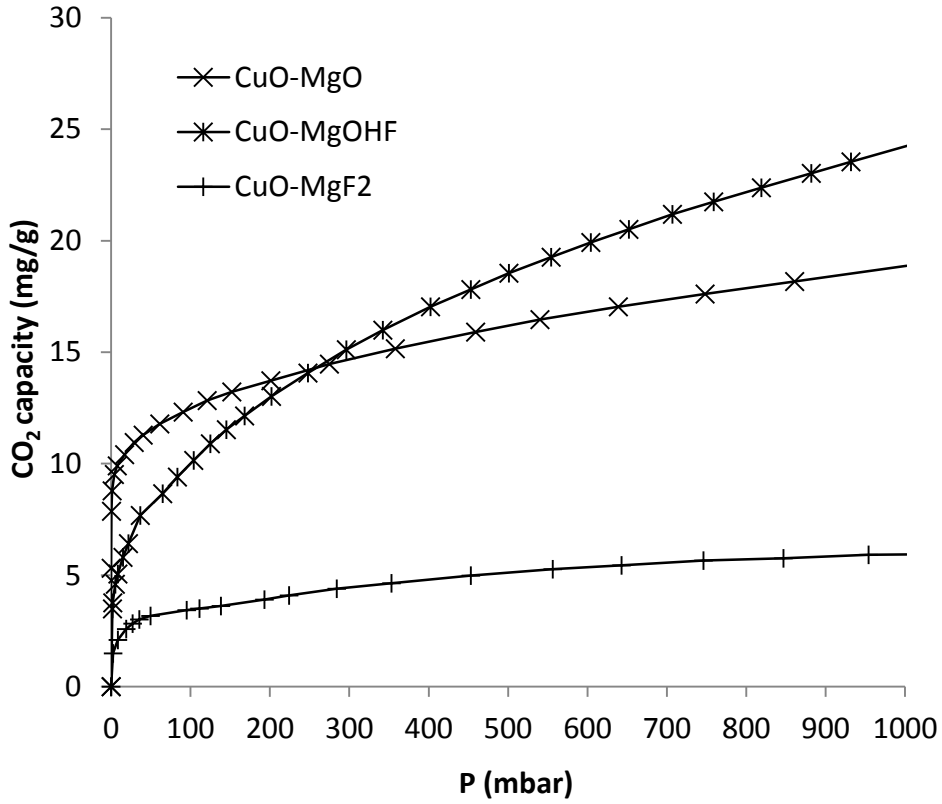

Figure 4: CO_2 monolayer content versus surface area for Cu-MgO, Cu-MgF(OH) and Cu-MgF_2

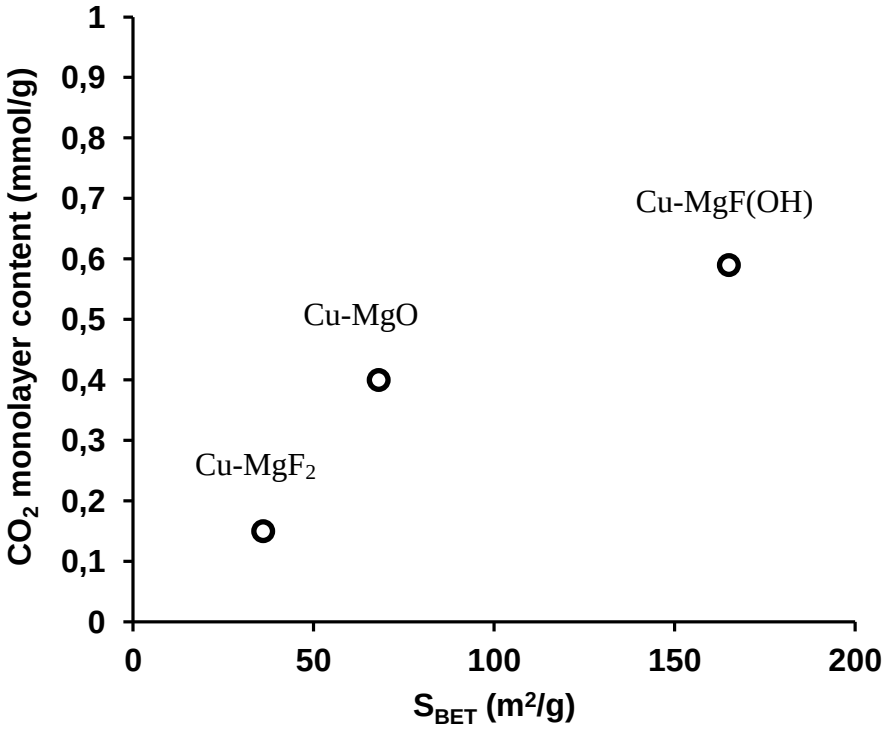

Figure 5: XPS analysis of Cu-MgO, Cu-MgFOH and Cu-MgF_2

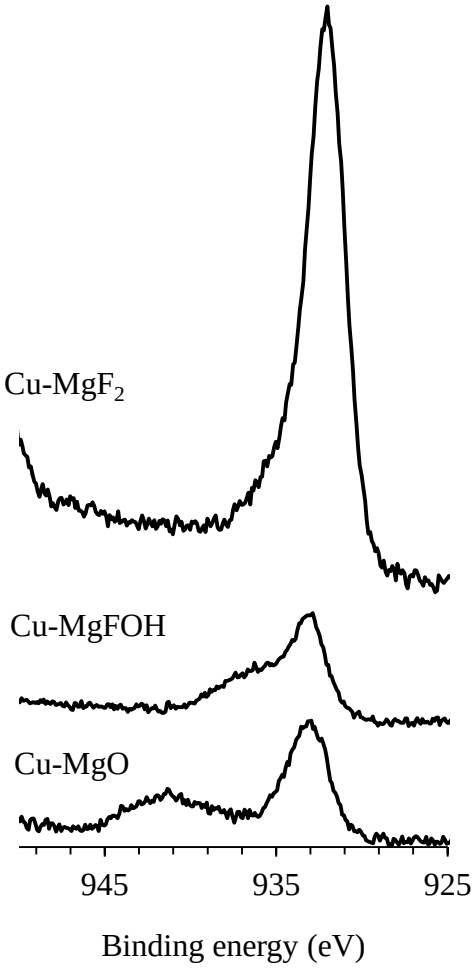

Figure 6: Glycerol conversion as a function of reaction time and catalyst

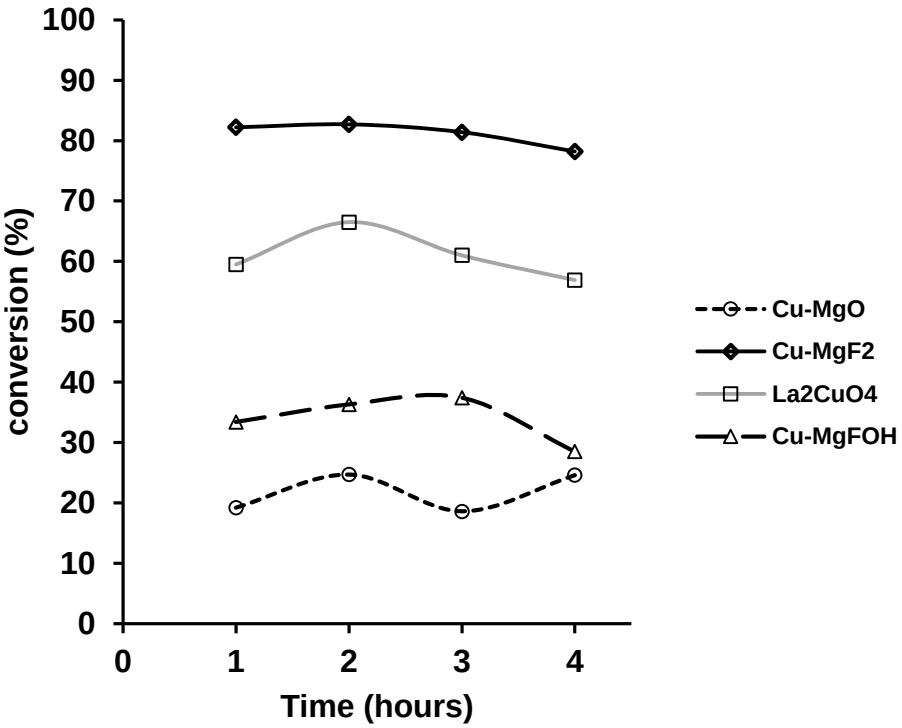

Figure 7: Yield in HA as a function of reaction time and catalyst

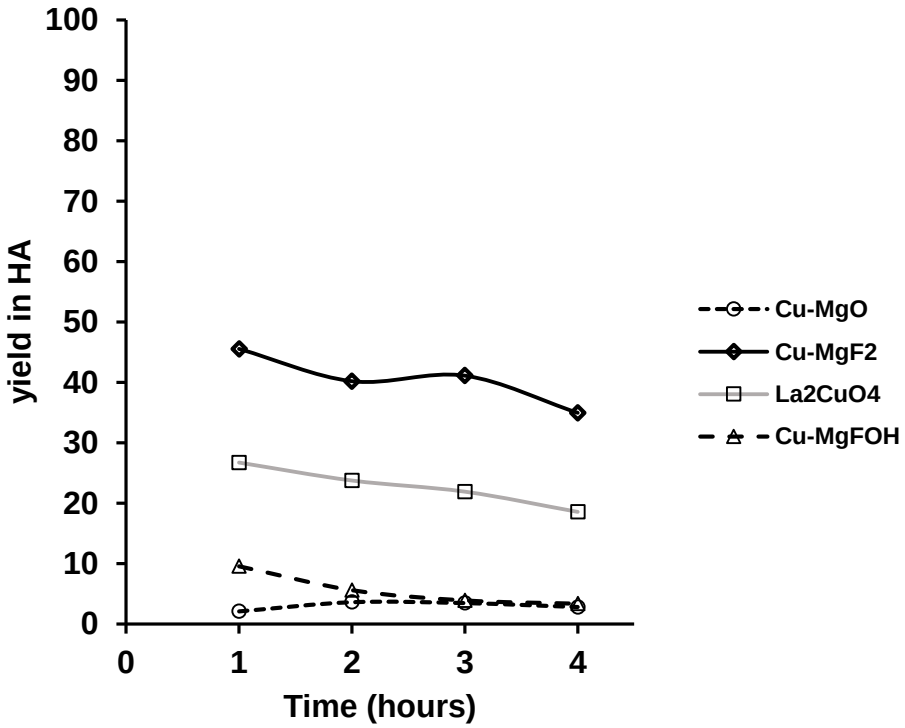

Figure 8: Hydroxyacetone yield after 1 hour of reaction as function of acid sites density and Cu^{+1} concentration

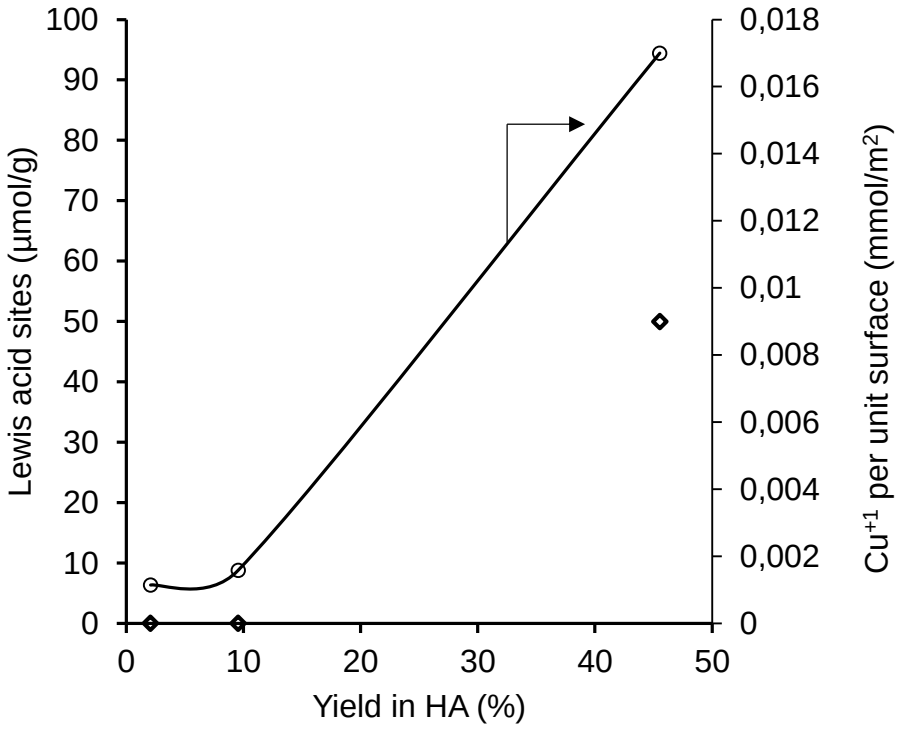

Figure 9: Proposed reaction routes of hydroxyacetone formation from glycerol on Cu-MgF_2 (a) Lewis acid mechanism proposed by Alhanash; (b) homolytic dissociation mechanism

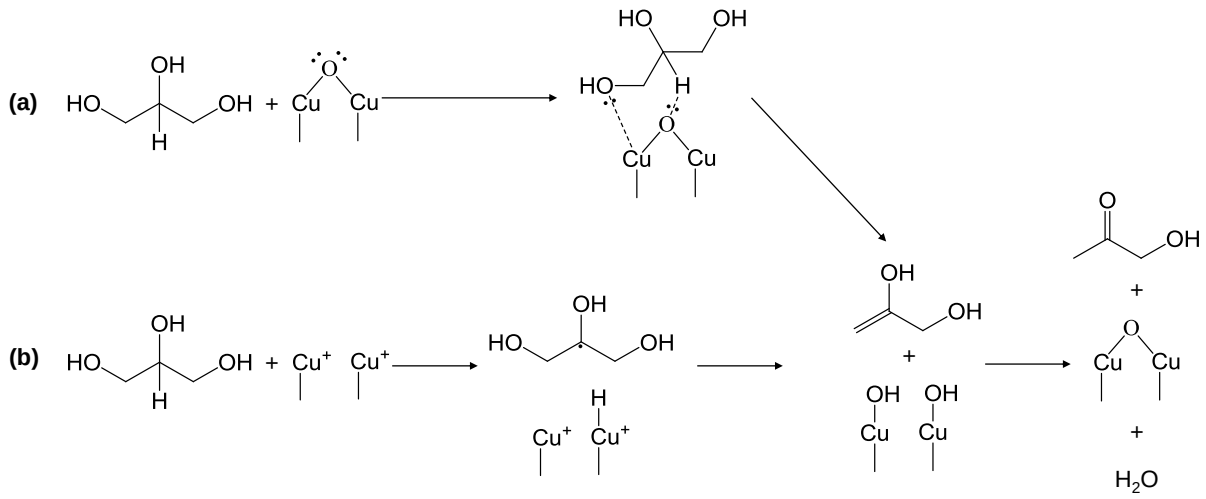

Figure 10: Potential energy plot for the reaction of neutral glycerol to form acetol (red: Nimos et al. [61], black: calculated Gibbs energy for mechanism b)

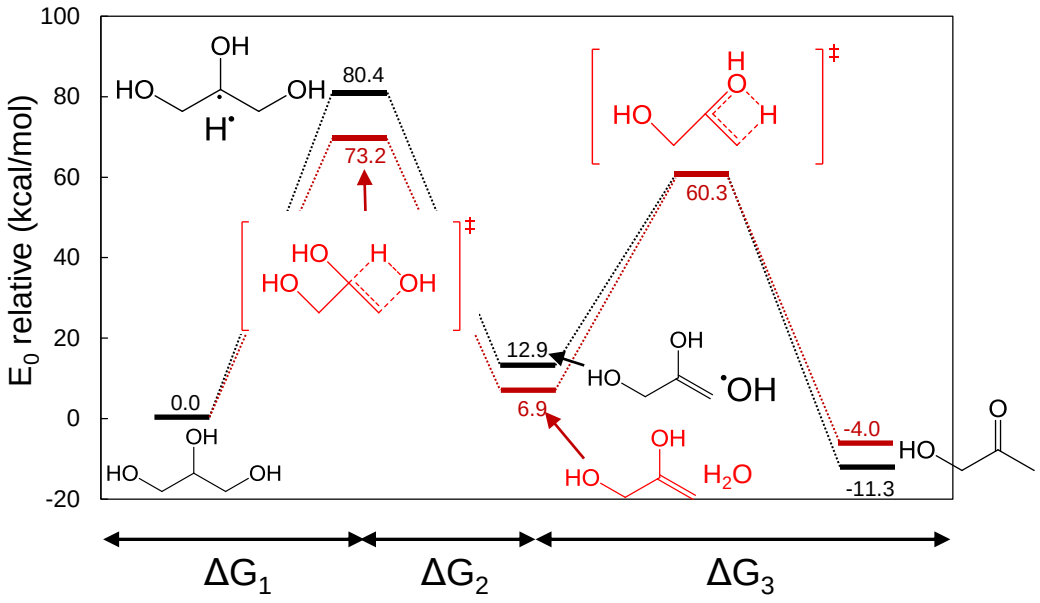

Figure 11: TGA curves of a) Cu-MgO, b) Cu-MgF(OH) and c) Cu-MgF_2 before (solid line) and after (dotted line) catalytic tests.